Journal of
Materials Chemistry C

Accepted Manuscript

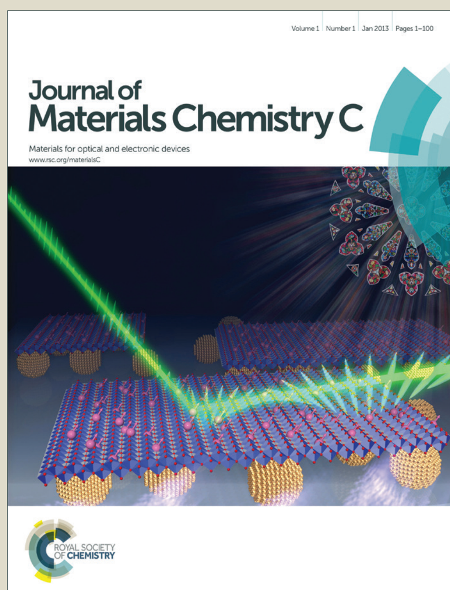

This is an *Accepted Manuscript*, which has been through the Royal Society of Chemistry peer review process and has been accepted for publication.

Accepted Manuscripts are published online shortly after acceptance, before technical editing, formatting and proof reading. Using this free service, authors can make their results available to the community, in citable form, before we publish the edited article. We will replace this *Accepted Manuscript* with the edited and formatted *Advance Article* as soon as it is available.

You can find more information about *Accepted Manuscripts* in the Information for Authors.

Please note that technical editing may introduce minor changes to the text and/or graphics, which may alter content. The journal's standard Terms & Conditions and the Ethical guidelines still apply. In no event shall the Royal Society of Chemistry be held responsible for any errors or omissions in this *Accepted Manuscript* or any consequences arising from the use of any information it contains.

ROYAL SOCIETY
OF CHEMISTRY

www.rsc.org/materialsC

Journal Name RSCPublishing

ARTICLE

Epitaxial Lateral Overgrowth of AlN on Self-Assembled Patterned Nanorods

Cite this: DOI: 10.1039/x0xx00000x

Michele Conroy[1,2,3,4], Vitaly Z Zubialevich[1], Haoning Li[1,3], Nikolay Petkov[1,4], Justin D Holmes[1,2,4*], Peter J Parbrook[1,3*]

Received 00th January 2012,
Accepted 00th January 2012

DOI: 10.1039/x0xx00000x

www.rsc.org/

We report an inexpensive nanoscale patterning process for epitaxial lateral overgrowth (ELOG) in AlN layers grown by metal organic vapour phase epitaxy (MOVPE) on sapphire. The pattern was produced by an inductively coupled plasma etch using a self-assembled monolayer of silica spheres on AlN as the lithographic mask. The resulting uniform 1 µm length rod structure across a wafer showed a massive reduction in threading dislocations (TDs) when annealed at 1100 °C. Overgrowing homoepitaxial AlN on top of the nanorods, at a temperature of 1100 °C, produced a crack free coalesced film with approximately 4µm of growth, which is formed at a much lower temperature compared to that typically required for microscale ELOG. The improved crystal quality, in terms of TD reduction, of the AlN above the rods was determined by detailed weak beam (WB) electron microscopy studies and showed that the threading dislocation density (TDD) was greatly reduced, by approximately two orders of magnitude in the case for edge-type dislocations. In-situ reflectance measurements during the overgrowth allowed for thickness coalescence to be estimated along with wafer curvature changes. The in-situ measurements also confirmed that tensile strain built up at a much slower rate in the ELOG AlN layer compared to that of AlN prepared directly on sapphire.

Introduction

AlN films possess a number of attractive properties including high thermal conductivity, wide band-gap, high chemical resistance and physical robustness.[1-3] The epitaxial growth of AlN buffer layers on heterosubstrates, such as sapphire, is an essential step in the advancement of deep ultra-violet (UV) based light emitting diodes (LEDs).[4] AlN is widely used as the basic template for most UV LEDs due to its UV transparency and small lattice mismatch to high Al% AlGaN, the alloy used for UV light emitting p- and n- layers as well as the active region in quantum wells[5, 6]. However the large lattice mismatch between AlN and sapphire and the low surface mobility of Al results in dislocations at this interface of the order 10^{10}cm^{-2}. Dislocations act as non-radiative recombination centres leading to a decreased internal quantum efficiency in the active region of LEDs[7, 8]. In order to achieve internal quantum efficiencies of above 50 % for deep UV LEDs, as compared to their visible InGaN-based LED counterparts currently on the market, the threading dislocation density (TDDs) would have to be <10^9cm^{-2} in the quantum well.[9] Essentially the AlN buffer layer needs to have a very low TDD so that very few dislocations reach the subsequent active region. Engineering the growth conditions such as pulsed-flow [10, 11] and migration enhanced MOVPE (MEMOVPE) [12, 13] have been used to reduce TDDs affecting mostly the screw type dislocations. In-situ MOVPE growth engineering has little effect however on the edge and mixed

Journal of Materials Chemistry C Accepted Manuscript

type dislocations. Hence alternative solutions capable of decreasing screw, edge and mixed TDs are required.

ELOG has been a long established method employed to decrease TDDs in GaN[14], permitting the realisation of efficient UV LEDs.[5, 6] There have been several different approaches to ELOG patterning templates, with the micron-stripe template the most common [15, 16] achieving significant reductions in the TDD, as highlighted by Imura et al [17]. As investigated by Kueller et al [18], a smooth crack free overgrown AlN layer can only be formed when the stripes are orientated in the (1-100) direction. Whereas the (11-20) direction will give a strongly faceted surface, leading to inhomogeneous Al distribution in AlGaN layers grown subsequently in UV LED devices. The orientation requirements for this patterning demands a high level expertise in expensive lithography alignment and additional processing steps. Also, growth on these micron scaled patterns is done under high temperatures, usually >1300 °C, necessary for Al mobility across the surface, resulting in higher power consumptions and higher running costs for the reactor.

Secondly the minimum coalescence thickness to produce smooth surfaces of AlN was in the order of > 4 μm.[15, 19] This extended growth thickness for ELOG at microscale ridge templates, greatly increases the epitaxy time and cost. Dong *et al.* [20] have approached these two issues by patterning at the nanoscale using a self-assembly method instead of the traditional method. Although they have overcome the orientation concern, there is only a slight decrease in coalescence thickness to ~3 μm. In comparison this article describes the development of a nanoscale self-assembly method of ELOG with a more rapid coalescence thickness, additionally we have reduced the number of processing steps by half to produce a suitable low defect density AlN ELOG template.

Experimental

AlN films were grown on c-plane sapphire substrates (0.38° ± 0.02° miscut towards the m-plane) using an Aixtron close coupled showerhead 3 × 2” MOVPE reactor. As presented in our previous work[21], a three step temperature variation recipe was used to grow the films to a thickness of 2 μm in the MOVPE reactor. The 2” AlN wafers were cut into halves for subsequent processing. The film was then patterned with a monolayer of silica spheres. The spheres were synthesised by the Stöber method[22] in ethanol to a diameter of 323 nm ± 5 nm. Before patterning a solution was made up of the silica spheres in ethanol at 10 % w/v and chloroform at a ratio of 2:3 and stirred for 30 min. This mixture was then introduced to the surface of a trough of water by a glass dropper with the film already submerged as previously described by Oh *et al.*[23] The glass trough was then lowered mechanically allowing the self-assembly of the silica particles onto the emerging wafer piece. Figure 1(b) shows surface images of a silica nanosphere-coated AlN film obtained by scanning electron microscopy (SEM) (FEI Helios NanoLab 600 Dual Beam SEM/FIB). The silica spheres assembled in a uniform hexagonally close packed pattern across the entire wafer as a monolayer.[24]

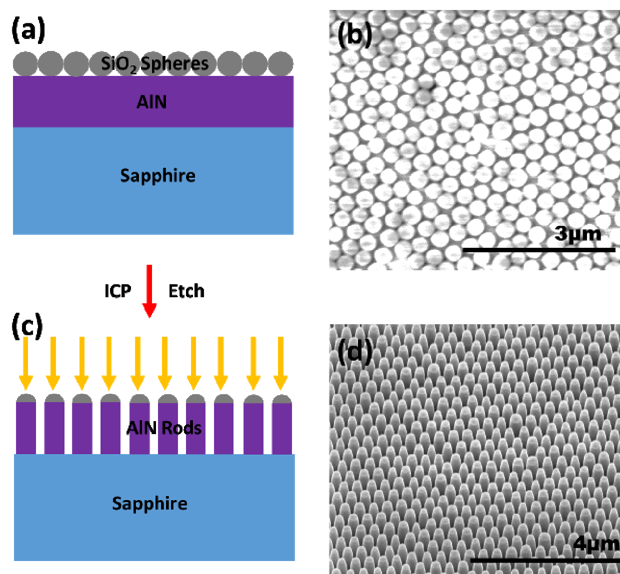

Figure 1. (a) Schematic side view of a silica sphere monolayer self-assembled on top of a AlN film grown on sapphire, (b) top down SEM image of the silica spheres self-assembled in a hexagonal two dimensional lattice monolayer, (c) schematic side view of newly formed AlN nanorods after ICP etch and (d) tilt view SEM image of the nano-rod structures.

Chlorine based inductively coupled plasma ICP dry etching was used to transfer the pattern into the underlying AlN film forming the structures shown in Figure 1 (d). The mean diameter of the nanorods formed was 330 nm ± 5 nm at their base and 170 nm ± 10 nm at their tops, with lengths around 1μm μm. The remaining silica mask after etching was removed by soaking the film in a bath of BOE (Ammonium fluoride – hydrofluoric acid mixture) for 5 min to ensure a silica-free surface before placing the film back in the reactor. Epitaxial lateral overgrowth was carried out on the patterned AlN/sapphire templates at a growth temperature of 1100 °C for 190 min giving an overgrowth thickness of ~4μm. The aluminum source used for the overgrowth layers was trimethylaluminum (TMAl), the nitrogen source was ammonia (NH_3), and H_2 as the carrier gas. For the overgrowth layer the V/III ratio was held at 50 and the reactor pressure at 50 mbar. These conditions were essentially the same as used for our thick planar AlN deposition.[21] For comparison two nanorod samples (no overgrowth) were also annealed in the reactor at 1100 °C under a flow of NH_3. In-situ reflectance measurements were carried out using a Laytec EpiTT system to monitor the growth. The susceptor surface temperature was measured by a pyrometer and compared to the spot measurements using an ARGUS CCS Pyrometric Profiling System multi-channel pyrometer for more accurate representation of the surface temperature variation during growth.

Journal of Materials Chemistry C Accepted Manuscript

 This journal is © The Royal Society of Chemistry 2012

SEM was utilised to obtain a visual representation of the overgrowth surface and for a comparison to the in-situ measurements. The surface morphology was confirmed through examination of the wafer piece using Nomarski interference optical microscopy additionally to high resolution surface SEM and cross sectional TEM scans. Crystal structure and defect analysis was undertaken on all samples using a JEOL 2100 200kV high resolution transmission electron microscope (TEM). Cross sectional TEM specimens were prepared with a focused ion beam (FIB) using a FEI HELIOS NanoLab 600 dual-beam system. The type and density of the TDs were investigated by weak beam dark field TEM imaging. Due to the limited field of view of our TEM in this mode, image stitching was required leading to contrast lines that can be seen in some of the images presented. For detailed analysis of the dislocation movement within the crystal structure the sample was cut in the (10-10) and (11-20) zone axes. The samples were then tilted to a 2 beam condition in the g = (11-20) and g = (10-10) directions respectively, where only the edge and mixed (edge and screw) type dislocations were visible. All samples were tilted in the (0002) direction to make only screw type dislocations visible for TDD determination. To estimate the TDD specimen foil thickness was measured in the SEM at the time of preparation using the FIB. Using this and the cross sectioned length examined in the TEM, the volume of material (or the effective cross-sectional area of the top surface) can be calculated, allowing the TDD to be estimated from the number of dislocations intercepting the top surface of the sample.

Results and Discussion

Fully coalesced AlN layers were achieved by overgrowth onto the nanorod patterned AlN templates, as presented in the diagram of figure 2. Figures 2 (a) and (b) show a cross-sectional SEM image of a nanorod AlN substrate overgrown at 1100 °C. This overgrowth produced a smooth crack free surface across an entire half 2" wafer piece as seen figures 2 (c)-(f). There were no cracks seen along the wafer edge as in figure 2 (c) typical for bulk AlN growth at 4μm thickness by MOVPE. The entire half wafer piece appeared smooth and uniform throughout as observed under Normarski interference optical microscope images, figure 2 (c) and (e). SEM scans as in figure 2 (d) confirmed the smooth top surface seen by optical microscopy and were additionally backed up by HR TEM micrographs, figure 2(f). In contrast to the AlN ELOG conditions reported elsewhere, where the growth temperature was > 1400 °C [6, 15], here the optimal growth temperature was much lower at 1100 °C. When higher temperatures were used for overgrowth (>1200°C) films with very rough surface morphology across the wafer piece were produced, indicating that some form of parasitic growth is occurring. The higher temperature is normally required for the activation and mobility of Al-containing species at the surface to enhance the mass transport over micron-sized patterns [25]. Herein we used nanoscale rod patterns that allowed a more efficient mass transport of reactants, realising faster overgrowth at a lower temperature. Additionally steps formed at the coalescence boundary typical of ELOG strategies was not an issue for this nanopatterning technique, as the air gaps were ~150 nm far less than the usual several micron air gaps used.

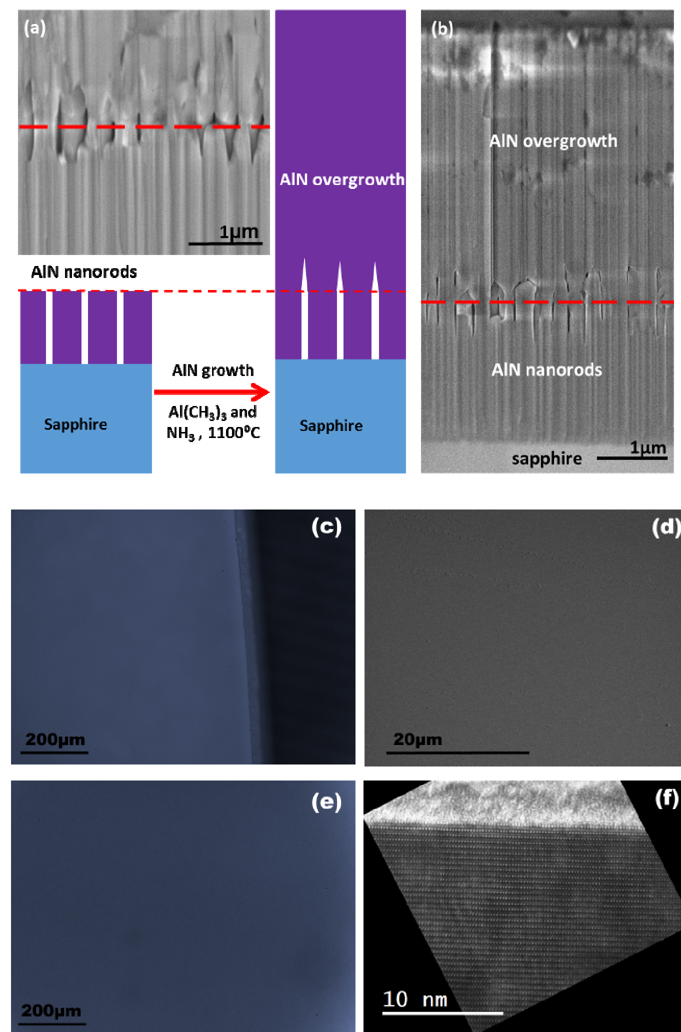

Figure 2. Representation of the AlN overgrowth on the rods, (a) SEM cross sectional scan of the AlN nanorod overgown layer interface with air gaps clearly visible and (b) SEM cross sectional scan of the entire AlN layers on sapphire, (c) Normarski interference optical microscope image of the wafer edge showing no visible cracks , (d) SEM scan of the top surface and (e) Normarski interference optical microscope image of the middle of the wafer piece both showing a smooth flat top surface, (f) HR TEM image of the top surface of the AlN layer.

From in-situ monitoring of the 650 nm reflection, as shown in figure 3(a), the growth oscillations are clearly visible and an increase of reflectance can be observed before coalescence, saturating at approximately 90 min of vertical growth, indicative of a smooth surface being obtained. As in other studies of AlN ELOG, growth may occur either on rod tops or parasitic growth in the gaps between the nanorods.[5] The lateral growth eventually encases voids as shown in figure 2, halting the parasitic growth. The coalescence rate is rapid as seen in the reflectance recovered in-situ measurements and the short void lengths above the overgrowth interface in SEM scans with

Journal of Materials Chemistry C Accepted Manuscript

the minimum coalescence thickness less than half compared to the thinnest reported in AlN ELOG high crystal quality layers.[20] The initial reflectance of the two wavelengths (405 and 650 nm) is very different when compared to a planar AlN film grown under the same growth conditions, because the interaction of the light with the 3 dimensional nanopatterning strongly depends on the wavelength. After 90 mins the 405 nm reflectance stays stable at 14.5 %, which is indicative of good AlN surface quality. The reduction in oscillation amplitude is caused by the spectral line width of the 405 nm LED source.

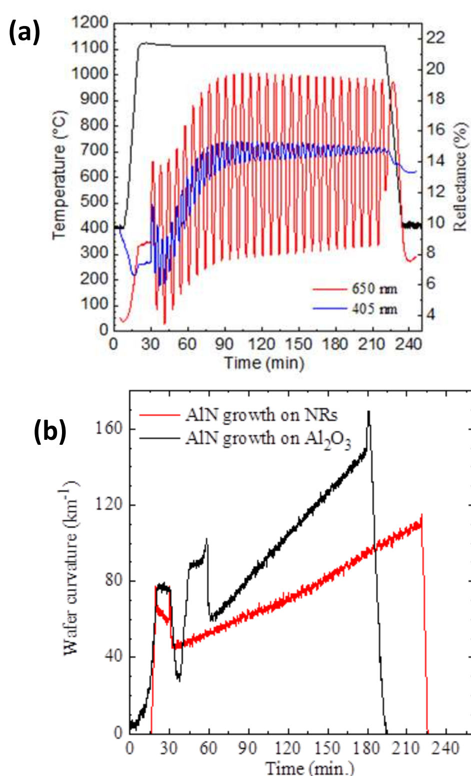

Figure 3. In-situ monitoring of AlN growth at 1100 °C. (a) The 650 nm and 405 nm light sources are used to measure reflectance % from the wafer in-situ, giving an indication of growth rate and morphological development in real time. The black line indicates temperature profile during growth. (b) In-situ monitoring of the wafer curvature variation throughout growth of AlN on sapphire compared to AlN on nanorods. The rise in the black line from t=60min and red line from t=45min represent material growth under identical conditions.

The growth of AlN on sapphire results in tensile strain in the AlN film as previously discussed. However this strain not only results in TD formation but also increases wafer curvature/bowing. The tensile strain is normally built up with increased AlN layer thickness, as shown in figure 3(b), where the black line shows the typical curvature increase for our optimal planar AlN on sapphire growth. As can be seen in the rate of curvature increase in figure 3 (b) where the rate of curvature increase is dramatically reduced when AlN is grown on the nanorods compared to the planar surface. Hence, the tension produced by the stress at the AlN-sapphire interface can be relieved substantially through homoepitaxial growth onto nanorods, allowing for thicker AlN to be grown without cracking of the wafer; often observed around the wafer edge in thicker material prepared conventionally. Typically planar AlN will start to exhibit edge cracking for thickness of ~3μm, where our growth on nanorods shows no cracking despite the overgrowth thickness of ~4μm and overall cumulative thickness of AlN on sapphire of ~6μm.

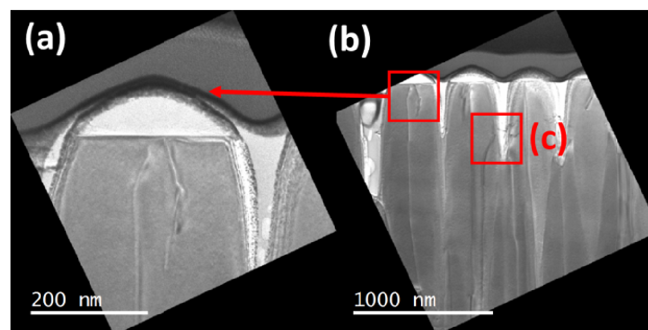

Figure 4. TEM cross sectional images of the nanorod template after ICP etch: (a) top of one rod, (b) lower magnification of (a) showing the other rods in the area.

A TEM investigation of the nanorod pattern was undertaken to fully understand the movement of the dislocations in the overgrown AlN layer. A nanorod sample after BOE treatment was prepared for TEM in the (10-10) zone axis as seen in figures 4(a) and (b). Dislocations were observed in most of the rods reaching the top surface. Examination of 20 rods showed around 35 dislocations threading to the rod tops, giving an approximate density of 1.75 dislocations/rod.

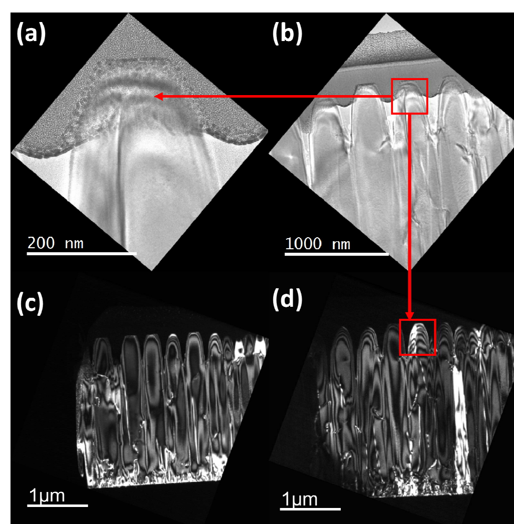

Figure 5. TEM images of an AlN nanorod template after ICP etch and annealing at 1100 °C under an ammonia flow: (a) and (b) BF images of a single rod with a dislocation reaching the surface, (c) and (d) sample tilted in the (0002) direction.

Journal of Materials Chemistry C Accepted Manuscript

This journal is © The Royal Society of Chemistry 2012

The nanorod template was then annealed at the same overgrowth temperature to see if there was any movement of the TDs. Figure 5 shows a visible reduction in the TDD of nanorod templated AlN film, with only one rod containing a dislocation reaching the top in the FIB cross section as shown in figure 5(a). A total of 25 rods were examined post-anneal and with the exception of the example described in Figure 5(a) they were all free of dislocations in their top half, examples of which can be seen in the bright field BF TEM image in figure 5(b) and in the weak beam dark field WBDF g-3g micrographs taken under g=0002 diffraction conditions, shown in figure 5(c) and (d). The termination of dislocations at the sidewalls appears to be a kinetically favourable option after supplying the crystal lattice with sufficient heat energy. The TEM studies confirm that the nano pattern itself is much more successful in providing a low TDD AlN template than previously reported in micron-scale ELOG.[15]

The dislocation free nature of semiconductor material, including III-Ns, in nanowire geometry is a well-established concept.[26, 27] The theory is based on the large surface to volume ratio found in nanowires that is very efficient in crystal strain relief.[28, 29] This lattice relaxation in nanowires allows for the production of near defect free III-N material not seen in heteroepitaxially grown 2-dimensional material. For our top down ICP etched nanorods dislocations will be immobile at the etch temperature. However during annealing in an ammonia atmosphere we can expect that the dislocations become sufficiently mobile to bend into the sidewall voids leading to an approximately 40-fold reduction in the dislocation density observed above; a reduction that is too large to be due to statistical variation across the sample. In figure 6 a schematic on the effect of annealing on three different dislocation paths is shown. Dislocations near the sidewall of the rod will be rapidly bent out in the air gap once there is sufficient thermal energy for them to move, shortening the dislocation length and hence reducing the total system energy. This effect can be expected to operate for the vast majority of dislocations including those near the centre of the rod, with only a few dislocations remaining, as illustrated by c_2 in figure 6.

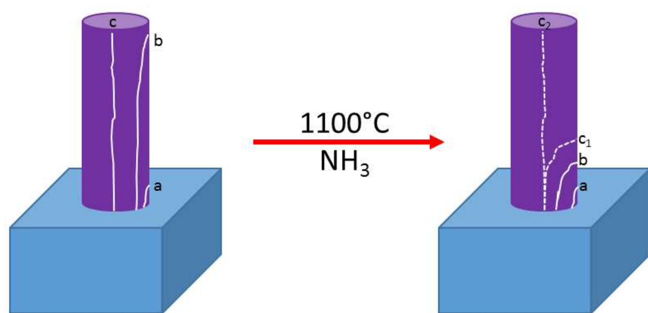

Figure 6. Schematic of the possible dislocation movements within the nanorods according to the distance from the centre of the rod and after treated with a high temperature anneal.

The detailed crystallographic information of overgrown AlN layers on AlN nanorods was observed using TEM in WBDF conditions. Two cross sections were cut out of the 1100 °C grown sample to observe the edge, screw and mixed type dislocations in the (10-10) and the (11-20) zone axes. Figures 7 and 8 show a TEM foil that is in the (10-10) zone axis. In figure 7(a) a weak beam (WB) g-3g micrograph taken under g = (11-20) diffraction conditions shows any edge and mixed type dislocations that may be present. Only one dislocation was observed to reach near to the top surface of the overgrown sample, seen at a higher magnification in image depicted in figure 7(d). The TDD of the coalesced AlN films were compared to optimised 3-step AlN grown layers previously obtained.[21] Without nanorod patterning the observed density of the edge and mixed dislocations was typically found to be ~4.4 $\times 10^{9}$ cm^{-2}, as highlighted in the image shown in figure 7(b). In comparison, AlN films produced using the nanorod ELOG process had TDDs of $< 10^{8}$ cm^{-2}, as highlighted in the TEM image shown figure 7(a). As discussed previously, reducing the edge dislocations cannot be done by in-situ growth engineering as with screw type dislocations. The nanoscaled ELOG presented here provides a definite reduction by more than two orders of magnitude of edge type dislocations.

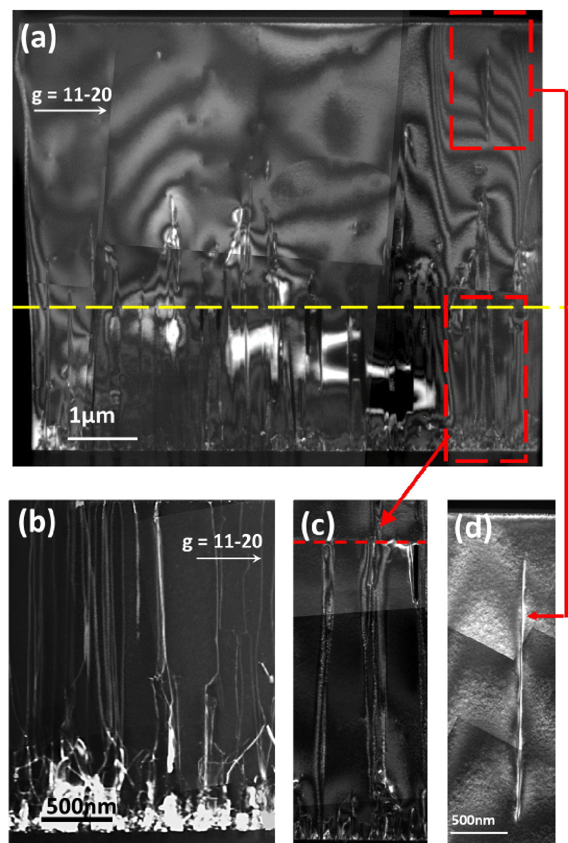

Figure 7. TEM images cut in the (10-10) zone axis: (a) FIB section of AlN overgrowth at 1100 °C tilted to g = (11-20) showing the a+c type dislocations with (c) and (d) showing dislocations at higher

Journal of Materials Chemistry C Accepted Manuscript

magnifications, (b) FIB cross sections of typical high quality 3 step AlN templates in the g = (11-20) without ELOG.

Tilting the same sample in the (0002) direction visualises any screw-type dislocations present in the cross sectioned foil as seen in figure 8(a). There are 8 screw type dislocations highlighted in the foil, calculated to represent a TDD of ~ 3 × 10^8 cm^{-2}. When compared to the screw type dislocation density of 1.5 × 10^9 cm^2 for 3-step grown AlN films, see figure 7(b), it is evident that the nanoscale ELOG patterning is successful in reducing the TDD of screw type significantly. These crystallographic results are backed up when another cross section was cut in the (11-20) zone axis giving similar results in the TDD, as seen in figure 9 below. The screw type density was estimated to be 3.5 × 10^8 cm^2 with no edge dislocations in the coalesced region, confirming once again the effectiveness of the approach in filtering out c-type dislocations.

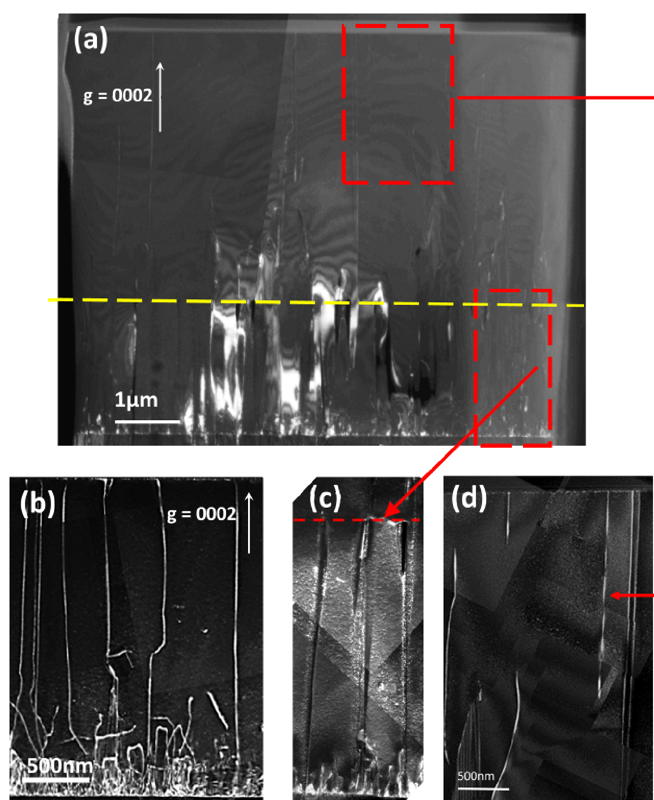

Figure 8. TEM images cut in the (10-10) zone axis: (a) FIB section of AlN overgrowth at 1100 °C tilted to g = (0002) showing the a type dislocations with (c) and (d) showing dislocations at higher magnifications, (b) FIB cross sections of typical high quality 3 step AlN templates in the g = (0002) without ELOG.

Compiling the entire crystallographic defect data obtained for both the AlN nanorod samples and the AlN coalesced samples provided a comprehensive description of the dislocation movement in the films. The annealed template before growth gave a near defect free surface for subsequent AlN homoepitaxy. However for the overgrown layer on this nanorod template there still are screw dislocations reaching the top surface. Figures 9(a) and (b) are cross sectional WBDF TEM images of the overgrown sample cut in the (11-20) zone axis, tilted to g = (0002) and g = (10-10) respectively near the point of minimum coalescence thickness. In figure 9 (y) and (z) orientations, both the screw and edge-type dislocations bend towards the voids in between the nanorods annihilating as previously discussed. However the shear stress at the minimum point of coalescence can result in lattice strain producing a screw dislocation as seen in figure 9(x). Hence dislocations reaching the top were mainly as a result of this formation.

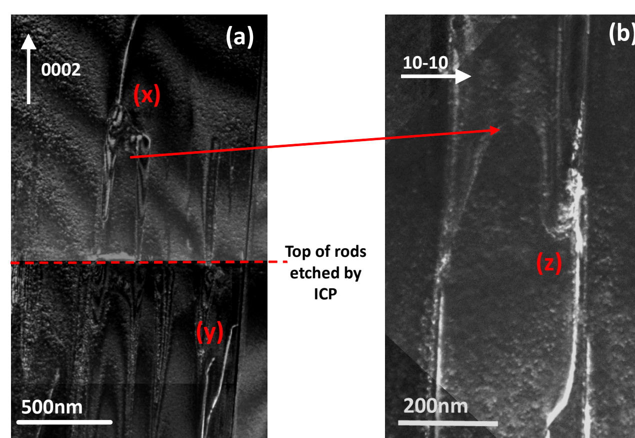

Figure 9. TEM images cut in the (11-20) zone axis: (a) FIB cross section of AlN overgrowth at 1100 °C and tilted to g = 0002, at (x) screw TD formed and (y) annihilation of screw TD highlighted. Image (b) of the same sample tilted to g = 10-10 showing the a+c type dislocations.

The overgrowth and dislocation behaviour in micron and nanoscale ELOG is explained in detail by the diagrams in Figure 10. The dislocations above the terrace on a micron scale propagate through the overgrowth layer to the surface above, as illustrated by the red region in figure 10 (a). The advantage of the nanoscale ELOG is that even the dislocations in the centre of the rod do not have a long distance to bend into the voids between the rods. The entire original ALN nanorod patterned wafer has been filtered of dislocations to a negligible number, instead of only stripes of TDD reduction in micron scale ELOG. As described above the majority of the TDD reaching the top surface of the overgrowth is in fact formed at the minimum point of coalescence as in the stripe patterned ELOG highlighted in green in figure 10 (b). Unlike classic ELOG[30, 31], where this stripe pattern is on a micron scale resulting in bending angles of the TDs at 90^0, they instead bend at slight angles, illustrated in the schematics of figure 10; thought to be due to the nanometre scale of the air gaps and the rod diameters.[32]

This journal is © The Royal Society of Chemistry 2012
Journal of Materials Chemistry C Accepted Manuscript

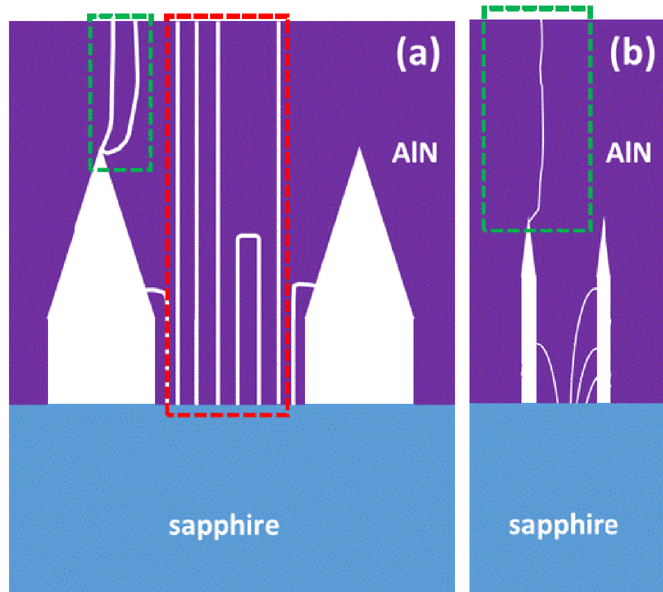

Figure 10. Schematic of the overgrowth on micron-scale ELOG (a) and (b) nanoscale ELOG.

Conclusion

In summary, a low defect density film of AlN has been grown heteroepitaxially on sapphire by MOVPE, using a nanopatterned lateral overgrowth technique. The self-assembly route to nanopatterning cut out several unnecessary processing steps typical in ELOG. The nanoscale ELOG technique described can achieve dislocations densities as low as 3.5×10^8 cm^2 in layers of our material at coalescence thickness <1.5μm. Due to the nano-structuring dislocations did not have as far to bend into the free space between the nanorods hence the reduction of TDD was uniform throughout the wafer. A much lower temperature of 1100 °C was implemented compared to temperatures of >1300 °C typically used for AlN coalescence, producing a smooth flat surfaces, with no evidence of significant steps on the overgrowth surface that can plague micron-scale ELOG methods. Nanorod template AlN film growth was recorded in real time by in-situ monitoring, showing the added benefit of decreased bowing of the wafer. The high crystal quality AlN template produced suggests the possibility of further low defect density heteropepitaxy growth and hence higher efficiency in end devices.

Acknowledgements

This research was enabled by the Irish Higher Education Authority Programme for Research in Third Level Institutions Cycles 4 and 5 via the INSPIRE and TYFFANI projects, and by Science Foundation Ireland (SFI) under Grant no. SFI/10/IN.1/I2993. PJP acknowledges funding from SFI Engineering Professorship scheme (07/EN/E001A) and MC acknowledges PhD research scholarship from INSPIRE. This work was conducted under the framework of the Irish Government's Programme for Research in Third Level Institutions Cycle 5, National Development Plan 2007-2013 with the assistance of the European Regional Development Fund. We also acknowledge the support of Dr.Mahbub Ahkter for his support with fabrication.

Notes and References

[1]*Tyndall National Institute, University College Cork, Lee Maltings, Dyke Parade, Cork, Ireland. E-mail: peter.parbrook@tyndall.ie*
[2] *Materials Chemistry & Analysis Group, Department of Chemistry, University College Cork, College Road, Cork, Ireland. E-mail: j.holmes@ucc.ie*
[3]*School of Engineering, University College Cork, College Road, Cork, Ireland.*
[4]*Centre for Research on Adaptive Nanostructures and Nanodevices (CRANN), Trinity College Dublin, Dublin 2, Ireland*

Journal of Materials Chemistry C Accepted Manuscript

1. K. Taylor and C. Lenie, *Journal of the Electrochemical Society*, 1960, **107**, 308-314.
2. W. Wang, W. Yang, Z. Liu, Y. Lin, S. Zhou, H. Qian, F. Gao and G. Li, *CrystEngComm*, 2014, **16**, 4100-4107.
3. H. Yang, W. Wang, Z. Liu and G. Li, *Journal of Physics D: Applied Physics*, 2013, **46**, 105101.
4. H. Hirayama, S. Fujikawa, N. Noguchi, J. Norimatsu, T. Takano, K. Tsubaki and N. Kamata, *physica status solidi (a)*, 2009, **206**, 1176-1182.
5. V. Kueller, A. Knauer, C. Reich, A. Mogilatenko, M. Weyers, J. Stellmach, T. Wernicke, M. Kneissl, Z. Yang, C. L. Chua and N. M. Johnson, *Photonics Technology Letters, IEEE*, 2012, **24**, 1603-1605.
6. A. A. Allerman, M. H. Crawford, S. R. Lee and B. G. Clark, *Journal of Crystal Growth*, 2014, **388**, 76-82.
7. K. Ban, J.-i. Yamamoto, K. Takeda, K. Ide, M. Iwaya, T. Takeuchi, S. Kamiyama, I. Akasaki and H. Amano, *Applied physics express*, 2011, **4**, 052101.
8. S. Y. Karpov and Y. N. Makarov, *Applied Physics Letters*, 2002, **81**, 4721-4723.
9. M. Kneissl, T. Kolbe, C. Chua, V. Kueller, N. Lobo, J. Stellmach, A. Knauer, H. Rodriguez, S. Einfeldt and Z. Yang, *Semiconductor Science and Technology*, 2011, **26**, 014036.
10. H. Hirayama, T. Yatabe, N. Noguchi, T. Ohashi and N. Kamata, *Applied Physics Letters*, 2007, **91**, -.
11. J. P. Zhang, M. A. Khan, W. H. Sun, H. M. Wang, C. Q. Chen, Q. Fareed, E. Kuokstis and J. W. Yang, *Applied Physics Letters*, 2002, **81**, 4392-4394.
12. R. S. Qhalid Fareed, J. P. Zhang, R. Gaska, G. Tamulaitis, J. Mickevicius, R. Aleksiejunas, M. S. Shur and M. A. Khan, *physica status solidi (c)*, 2005, **2**, 2095-2098.
13. R. Jain, W. Sun, J. Yang, M. Shatalov, X. Hu, A. Sattu, A. Lunev, J. Deng, I. Shturm, Y. Bilenko, R. Gaska and M. S. Shur, *Applied Physics Letters*, 2008, **93**, 051113-051113-051113.
14. K. Hiramatsu, *Journal of Physics: Condensed Matter*, 2001, **13**, 6961.
15. V. Kueller, A. Knauer, F. Brunner, U. Zeimer, H. Rodriguez, M. Kneissl and M. Weyers, *Journal of Crystal Growth*, 2011, **315**, 200-203.
16. U. Zeimer, V. Kueller, A. Knauer, A. Mogilatenko, M. Weyers and M. Kneissl, *Journal of Crystal Growth*, 2013, **377**, 32-36.
17. M. Imura, K. Nakano, G. Narita, N. Fujimoto, N. Okada, K. Balakrishnan, M. Iwaya, S. Kamiyama, H. Amano, I. Akasaki, T. Noro, T. Takagi and A. Bandoh, *Journal of Crystal Growth*, 2007, **298**, 257-260.
18. V. Kueller, A. Knauer, U. Zeimer, H. Rodriguez, A. Mogilatenko, M. Kneissl and M. Weyers, *physica status solidi (c)*, 2011, **8**, 2022-2024.
19. H. Hirayama, S. Fujikawa, J. Norimatsu, T. Takano, K. Tsubaki and N. Kamata, *physica status solidi (c)*, 2009, **6**, S356-S359.
20. P. Dong, J. Yan, J. Wang, Y. Zhang, C. Geng, T. Wei, P. Cong, Y. Zhang, J. Zeng, Y. Tian, L. Sun, Q. Yan, J. Li, S. Fan and Z. Qin, *Applied Physics Letters*, 2013, **102**, -.
21. H. Li, T. C. Sadler and P. J. Parbrook, *Journal of Crystal Growth*, 2013, **383**, 72-78.
22. W. Stöber, A. Fink and E. Bohn, *Journal of colloid and interface science*, 1968, **26**, 62-69.
23. J. R. Oh, J. H. Moon, S. Yoon, C. R. Park and Y. R. Do, *Journal of Materials Chemistry*, 2011, **21**, 14167-14172.
24. M. A. Conroy, N. Petkov, H. N. Li, T. C. Sadler, V. Zubialevich, J. D. Holmes and P. J. Parbrook, *ECS Transactions*, 2013, **53**, 39-42.
25. K. Nakano, M. Imura, G. Narita, T. Kitano, Y. Hirose, N. Fujimoto, N. Okada, T. Kawashima, K. Iida, K. Balakrishnan, M. Tsuda, M. Iwaya, S. Kamiyama, H. Amano and I. Akasaki, *physica status solidi (a)*, 2006, **203**, 1632-1635.
26. F. R. N. Nabarro, *Advances in Physics*, 1952, **1**, 269-394.
27. R. Colby, Z. Liang, I. H. Wildeson, D. A. Ewoldt, T. D. Sands, R. E. García and E. A. Stach, *Nano Letters*, 2010, **10**, 1568-1573.
28. P. Deb, H. Kim, V. Rawat, M. Oliver, S. Kim, M. Marshall, E. Stach and T. Sands, *Nano Letters*, 2005, **5**, 1847-1851.
29. G. Avit, K. Lekhal, Y. André, C. Bougerol, F. Réveret, J. Leymarie, E. Gil, G. Monier, D. Castelluci and A. Trassoudaine, *Nano Letters*, 2014, **14**, 559-562.
30. P. Vennéguès, B. Beaumont, V. Bousquet, M. Vaille and P. Gibart, *Journal of Applied Physics*, 2000, **87**, 4175-4181.
31. Z. Liliental-Weber, M. Benamara, W. Swider, J. Washburn, J. Park, P. A. Grudowski, C. J. Eiting and R. D. Dupuis, *MRS Online Proceedings Library*, 1998, **537**, null-null.
32. J. Bai, T. Wang, P. J. Parbrook and A. G. Cullis, *Applied Physics Letters*, 2006, **89**, -.

Journal of Materials Chemistry C Accepted Manuscript

This journal is © The Royal Society of Chemistry 2012